

THE NEAR-INFRARED BACKGROUND: INTERPLANETARY DUST OR PRIMORDIAL STARS?

ELI DWEK,¹ RICHARD G. ARENDT,² AND FRANK KRENNRICH³

Received 2005 April 19; accepted 2005 August 27

ABSTRACT

The intensity of the diffuse $\sim 1\text{--}4\ \mu\text{m}$ sky emission from which solar system and Galactic foregrounds have been subtracted is in excess of that expected from energy released by galaxies and stars that formed during the $z \lesssim 5$ redshift interval. The spectral signature of this excess near-infrared background light (NIRBL) component is almost identical to that of reflected sunlight from the interplanetary dust cloud and could therefore be the result of the incomplete subtraction of this foreground emission component from the diffuse sky maps. Alternatively, this emission component could be extragalactic. Its spectral signature is consistent with that of redshifted continuum and recombination line emission from H II regions formed by the first generation of very massive stars. In this paper we analyze the implications of this spectral component for the formation rate of these Population III stars, the redshift interval during which they formed, the reionization of the universe, and evolution of collapsed halo masses. Assuming that these Population III stars are massive objects radiating at the Eddington luminosity and ending their lives by directly collapsing into black holes, we find that to reproduce the intensity and spectral shape of the NIRBL requires a peak star formation rate of $\sim 2.5 M_{\odot} \text{ yr}^{-1} \text{ Mpc}^{-3}$, with a $(1+z)^{-2}$ dependence on redshift, until the epoch ends at redshifts $z \approx 7\text{--}9$. It requires a comoving luminosity density of about $2.7 \times 10^{11} L_{\odot} \text{ Mpc}^{-3}$, corresponding to a total energy input of 670–820 keV per baryon, and that about 10% of the total number of baryons in the universe be converted to Population III stars. All these numbers are higher by about a factor of 4–10 than those derived from models in which Population III stars form at a rate that is proportional to the collapse rate of halos in a cold dark matter dominated universe. Furthermore, an extragalactic origin for the NIRBL leads to physically unrealistic absorption-corrected spectra of distant TeV blazars. All these results suggest that Population III stars contribute only a fraction of the NIRBL intensity, with zodiacal light, star-forming galaxies, and/or nonnuclear sources giving rise to the remaining fraction. Further 0.1–10 μm observations of the diffuse sky and the zodiacal cloud are therefore crucial for resolving the true spectrum and origin of the NIRBL.

Subject headings: cosmology: theory — diffuse radiation — early universe — galaxies: formation — infrared: general — stars: formation

1. INTRODUCTION

The extragalactic background light (EBL) consists of all radiative energy outputs, whether powered by nuclear or gravitational processes, that were released into the universe after the epoch of recombination. At UV to near-infrared wavelengths it comprises the fraction of that radiation that was not absorbed by dust and reradiated at mid- to far-infrared (IR) wavelengths. In addition to the radiative output from star-forming galaxies and active galactic nuclei, the EBL can also harbor the radiative imprint of a variety of exotic objects, including exploding stars, primordial black holes, decaying particles, and primordial very massive objects (Bond et al. 1986). Assuming that all the dark matter required to close the universe was contained in these objects, Bond et al. (1986) suggested that they could have an important effect on the spectrum of the EBL. However, subsequent limits on and detection of the EBL (Hauser et al. 1998; Hauser & Dwek 2001) strongly constrained the mass of some of these objects. Furthermore, the lack of any strong physical motivation for their existence rendered their contribution highly speculative.

Quasars offer an alternative method for probing the formation and evolution of the first collapsed objects in the universe. The

absorption spectra of high-redshift quasars can reveal the ionization state of the intergalactic medium (IGM) and therefore provide direct evidence for the presence or absence of ionizing sources at high redshifts. The absence of a Gunn-Peterson trough in the spectrum of the luminous quasar SDSS 1044–0125 located at $z = 5.8$ suggested that the universe was already highly ionized at that redshift (Fan et al. 2000). The detection of excess power in the polarization-temperature cross-power spectrum of the cosmic microwave background with the *Wilkinson Microwave Anisotropy Probe* (WMAP) at large angular scales confirmed that the universe was reionized at high redshifts (Bennett et al. 2003). Assuming that the reionization was instantaneous and complete, Kogut et al. (2003) derived an optical depth of $\tau \approx 0.17 \pm 0.4$ to reionization, corresponding to a redshift of $z = 17 \pm 3$. However, the earlier detection of a Gunn-Peterson trough in the spectra of several quasars with redshifts between ~ 5.8 and 6.3 (Fan et al. 2001) suggests that neutral hydrogen was present at those redshifts in sufficient quantities to lead to the absorption of all photons shortward of the Lyman limits from their spectra. These seemingly conflicting results suggest that the reionization of the universe did not occur in a single event, rendering the formation history and evolution of the first objects capable of producing ionizing radiation a question of great cosmological importance.

The formation of these first ionizing stars is relatively well understood, since it took place under conditions that are considerably simpler than those governing present-day star formation: a well-defined set of initial conditions needed to calculate the growth of dark matter density perturbations, a metal-free

¹ Observational Cosmology Laboratory, Code 665, NASA Goddard Space Flight Center, Greenbelt, MD 20771; eli.dwek@nasa.gov.

² Science Systems and Applications, Inc., Observational Cosmology Laboratory, Code 665, NASA Goddard Space Flight Center, Greenbelt, MD 20771; arendt@milkyway.gsfc.nasa.gov.

³ Department of Physics and Astronomy, Iowa State University, Ames, IA 50011-3160; krennich@iastate.edu.

gas, simplifying calculations of the chemistry and cooling of the collapsing baryonic matter, and the absence of magnetic fields (see recent reviews by Loeb & Barkana 2001; Barkana & Loeb 2001; Bromm & Larson 2004; Glover 2005; Kashlinsky 2005). In spite of this relative simplicity, there are still many unanswered questions regarding the formation and nature of these first stellar objects: (1) When did these objects first form, and when did they stop forming? (2) What is the fraction of the collapsing gas that actually formed stars? (3) How did the gas fragment, and what is the stellar initial mass function? (4) How did the ionizing stellar radiation interact with the ambient gas, and how did these primordial H II regions evolve?

Searches for answers to these questions have led to a flurry of models and predictions of various observational effects associated with these Population III stars, such as their effect on the early helium and metal enrichment of the universe (e.g., Haiman & Loeb 1997; Salvaterra & Ferrara 2003b; Scannapieco et al. 2003) or their anisotropies (Kashlinsky et al. 2004; Cooray et al. 2004; Magliocchetti et al. 2003). In particular, Santos et al. (2002, hereafter SBK02), Cooray & Yoshida (2004), and Madau & Silk (2005) reconsidered their potential imprint on the spectrum of the EBL. More recently, Salvaterra & Ferrara (2003a) claimed the actual detection of their signature in the $\sim 1\text{--}4\ \mu\text{m}$ wavelength region of the EBL.

The claimed detection of the Population III signature in the EBL relies on the *COBE* DIRBE (Hauser et al. 1998) and *IRTS* NIRS (Matsumoto et al. 2005) $1\text{--}4\ \mu\text{m}$ measurements, assuming their extragalactic origin. The DIRBE and NIRS residuals, obtained after the subtraction of local foreground emission components from the diffuse sky, are higher than the ground-based measurements of the integrated light from resolved galaxies (Madau & Pozzetti 2000) or even their extrapolated intensity based on the evolutionary models (Totani et al. 2001). The *Hubble Space Telescope* (*HST*) and ground-based optical detections of the EBL by Bernstein et al. (2002) are also in excess of their ground-based counterparts, but by a smaller amount. The near-IR ($\sim 1\text{--}4\ \mu\text{m}$) region of the EBL may therefore be a distinct spectral component that may be of either local or extragalactic origin.

In this paper we first describe the data and examine the nature of the excess emission component, whether it is truly extragalactic or whether it reflects systematic errors in the subtraction of foreground emission from the zodiacal dust cloud (§ 2). Assuming its extragalactic nature, we fit this component with the contribution of the line and continuum emission from metal-free Population III stars and their surrounding nebulae (§ 3). Our approach differs from that of SBK02 or Cooray & Yoshida (2004), who calculated the EBL expected from Population III stars forming at a predetermined rate inferred from the collapse and merging rate of dark matter halos. These studies did not attempt to fit the DIRBE or NIRS data, and consequently, their model predictions fall short of the excess $\sim 1\text{--}4\ \mu\text{m}$ emission. In contrast, Salvaterra & Ferrara (2003a) and Madau & Silk (2005) assumed that the excess emission is extragalactic and explored the possibility that it was formed by Population III stars. However, Salvaterra & Ferrara (2003a) failed to explore the implications of their model for the formation rate of these objects. Madau & Silk (2005) assumed all the stellar energy to be emitted as Ly α radiation and adopted a *very* conservative estimate for the $1.25\ \mu\text{m}$ NIRBL intensity of only $2.5\ \text{nW m}^{-2}\ \text{sr}^{-1}$, instead of the value of $\sim 70\ \text{nW m}^{-2}\ \text{sr}^{-1}$ implied by the observed excess and fitted by Salvaterra & Ferrara (2003a).

In our model we assume that the Population III stars form an ionization-bounded H II region, so that all their ionizing pho-

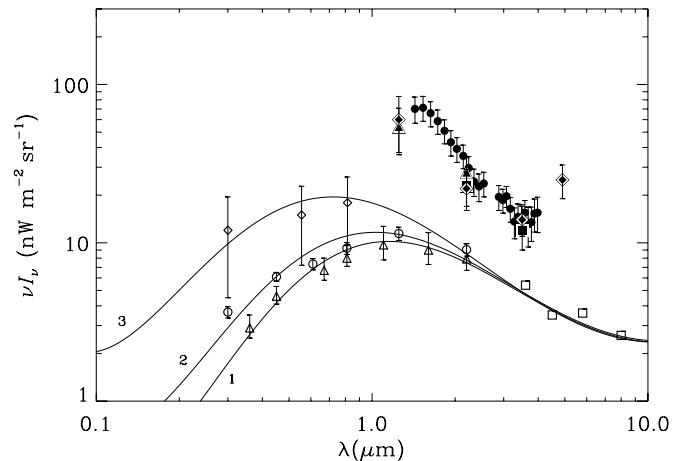


FIG. 1.—Limits and detections of the EBL. The three lines represent possible fits to the EBL spectrum generated by normal star-forming galaxies. The curve labeled “2” (EBL2) is the nominal EBL spectrum attributed to these galaxies in this paper. References to the observations are in the text.

tons are absorbed in the remaining nebular gas from which they were formed, instead of escaping into the IGM, and use *CLOUDY* to calculate the emerging stellar and nebular emission. Assuming a continuous star formation process over a given redshift interval, we calculate the spectral signature of these objects for a variety of model parameters. Fitting these spectra to the observations, we derive the epoch over which Population III stars formed, their formation rate, and the total energy released during their lifetime. Cosmological implications are presented in § 4. In § 5 we briefly describe other considerations that can shed light on the origin of the EBL, namely, fluctuations in the EBL and the effect of the NIRBL on the absorption-corrected spectra of blazars. The results of our paper are briefly summarized in § 6.

In all our calculations we adopt a cosmological model with parameters determined from the analysis of *WMAP* (Bennett et al. 2003): a dark energy density of $\Omega_\Lambda = 0.73$ and total and baryonic matter densities of $\Omega_m = 0.27$ and $\Omega_b = 0.044$, respectively. The densities are normalized to the critical density using a Hubble constant of $H_0 = 70\ \text{km s}^{-1}\ \text{Mpc}^{-1}$.

2. THE NATURE OF THE EXCESS BACKGROUND AT $1\text{--}5\ \mu\text{m}$

2.1. Observations

Figure 1 depicts the current limits and detections of the EBL in the $0.1\text{--}10\ \mu\text{m}$ wavelength region. These limits and detections were obtained by a variety of analyses and observational methods, including (1) ground- and space-based measurements of integrated galaxy light (Madau & Pozzetti 2000 [*open triangles*]; Bernstein et al. 2002 [*open diamonds*]), (2) direct measurements based on data obtained by the Diffuse Infrared Background Experiment (DIRBE) on board the *Cosmic Background Explorer* (*COBE*) satellite (Hauser et al. 1998; Dwek & Arendt 1998; Arendt & Dwek 2003 [*filled diamonds*]; Cambr sy et al. 2001 [*filled triangles*]; Wright & Reese 2000; Gorjian et al. 2000; Wright 2001 [*filled squares*]) and the Near-Infrared Spectrometer (NIRS) on board the *Infrared Telescope in Space* (*IRTS*; Matsumoto et al. 2005; *filled circles*), and (3) extrapolated galaxy number counts (Totani et al. 2001; *open circles*). The curves labeled “1,” “2,” and “3” in the figure are smooth polynomial fits representing three possible EBL spectra formed by star-forming galaxies: a maximal one, designated EBL1, fitted to the Bernstein et al. (2002) data; a minimal one, designated EBL3, fitted to the

lower limits defined by the galaxy number counts of Madau & Pozzetti (2000); and an intermediate one, designated EBL2, fitted to the Totani et al. (2001) points. These polynomial fits include mid- and far-IR limits and measurements by Infrared Array Camera (IRAC) instruments on board the *Spitzer Space Telescope* (Fazio et al. 2004 [*open squares*]; Metcalfe et al. 2003 [$15\ \mu\text{m}$]; Papovich et al. 2004 [$24\ \mu\text{m}$]; Lagache et al. 2000 [$100\ \mu\text{m}$]; Hauser et al. 1998 [$140, 240\ \mu\text{m}$]). Differences between the three backgrounds were found to be negligible beyond $\sim 10\ \mu\text{m}$.

The figure suggests that at $\sim 1\text{--}4\ \mu\text{m}$ the EBL intensity is higher than the integrated light from resolved galaxies (Madau & Pozzetti 2000) or even their extrapolated intensity based on the evolutionary models (Totani et al. 2001). We use the Totani et al. extrapolations as the baseline for the EBL intensity from normal galaxies and designate this EBL2 component as GEGL. Furthermore, as suggested by the figure, it seems hard to smoothly join the $\sim 1\text{--}4\ \mu\text{m}$ region of the EBL spectrum to that at shorter wavelengths while maintaining the general spectral shape of the integrated galactic starlight. Put differently, the GEGL formed by the unabsorbed stellar continuum emission, when normalized to fit the near-IR spectrum, requires an integrated $0.1\text{--}10\ \mu\text{m}$ EBL intensity of about $100\ \text{nW m}^{-2}\ \text{sr}^{-1}$ (Hauser & Dwek 2001). This value is considerably larger than the total radiative energy released from star-forming galaxies over the $z = 0\text{--}5$ redshift interval, which is only about $50\ \text{nW m}^{-2}\ \text{sr}^{-1}$ after the fraction of starlight that has been absorbed and reradiated by dust has been subtracted. The near-infrared background light (NIRBL), defined hereafter as the $\sim 1\text{--}4\ \mu\text{m}$ diffuse light from which the extragalactic component (GEGL) has been subtracted, is therefore a distinct spectral component with an integrated intensity $\gtrsim 30\ \text{nW m}^{-2}\ \text{sr}^{-1}$.

2.2. The Case for a Local Origin for the Emission

We start with some cautionary notes concerning the attribution of the excess DIRBE and IRTS emission to extragalactic sources. First, there have been only two space missions, *COBE* DIRBE (Hauser et al. 1998) and *IRTS* NIRS (Matsumoto et al. 2005), that have performed absolute measurements of the near-IR sky brightness over significantly large areas of the sky. The NIRS measurements are much more limited in time and area than the DIRBE observations, but the total measured sky brightness does match DIRBE. While it is very encouraging that these two experiments are in excellent agreement, it is still of great interest to have future experiments confirm these results with different instrumentation and under different circumstances.

Second, the extragalactic interpretation of the origin of the NIRBL hinges on the large discontinuity between the DIRBE and NIRS infrared measurements and the *HST*- and ground-based UV-optical determinations of the EBL by Bernstein et al. (2002). Systematic errors in acquisition and analyses of these data sets may produce just such a discontinuity. Clearly, further observations covering the $\sim 0.1\text{--}10\ \mu\text{m}$ wavelength region with good spectral resolution would be valuable in revealing the true nature of the NIRBL.

Third, extraction of the NIRBL depends on accurate removal of stellar and zodiacal foregrounds. The NIRBL appears to be only $\sim 10\%$ of the total near-IR sky brightness, so relatively small errors in the foregrounds may be significant. Hauser et al. (1998) did not claim detections of the NIRBL because the uncertainties in the foreground models were too large. Subsequent analyses (e.g., Arendt & Dwek 2003 and references therein) have aimed at reducing the uncertainties in the subtraction of foreground emissions.

In the near-IR there are two dominant foregrounds. (1) Galactic stars: Their emission can be empirically removed by constructing

spatial templates of the stellar emission (Dwek & Arendt 1998) or by integrating NIR star counts (from high-resolution observations) and subtracting the flux from the low-resolution DIRBE measurements at specific locations (Gorjian et al. 2000; Wright 2001; Cambresy et al. 2001). Both these methods are more robust than a statistical approach to the removal of the Galactic stellar foreground (Arendt et al. 1998). However, all these methods are susceptible to error if there exists a Galactic population of faint stars that have not been directly observed or used to constrain the statistical models. (2) Interplanetary dust particles: The strongest foreground to be removed is the zodiacal light produced by the scattering of sunlight by and thermal emission of interplanetary dust (IPD) particles. The zodiacal light is intrinsically diffuse, so, unlike the stellar foreground, it is not possible to resolve and subtract the individual sources regardless of spatial resolution and sensitivity. Most analyses of DIRBE and NIRS data have used the Kelsall et al. (1998) zodiacal light model or a closely related derivative (Hauser et al. 1998; Wright 1998; Wright & Reese 2000; Matsumoto et al. 2005). This zodiacal light model was fit to the observed temporal variation of the observations. Thus, the model is insensitive to any IPD component that is effectively isotropic and produces no significant variation in brightness over the range of elongation observed by DIRBE. Wright's versions of the zodiacal light model address this problem by placing some constraints in the mid-IR, but it is possible that there may be systematic errors in the model that affect the scattered light in the near-IR without affecting the thermal emission in the mid-IR. Components that are on a scale large enough to have small annual variations, or that are spherically distributed around the earth, such that they have no annual variation, may be overlooked.

There are several known spatial and temporal discrepancies between the Kelsall et al. (1998) model and the data. One, noticeable even at high ecliptic latitudes, is caused by the imperfect fitting of the earth-resonant ring and structures. Kelsall et al. (their Fig. 11a) show that at $12\ \mu\text{m}$ these errors can be up to 4% of the model intensity, which can lead to a 40% error in the EBL estimate at this wavelength. Another appears as a periodic residual with a period matching the solar rotation period. These residuals are found to be strongly correlated with daily measures of solar activity, such as the Mg II index and sunspot number (Kelsall et al. 1998; T. Kelsall 2005, private communication). It is unknown whether these variations occur in the zodiacal cloud or in the earth's exosphere. These variations represent only $\sim 2\%$ of the IPD intensity at 1.25 and $3.5\ \mu\text{m}$, but without an understanding of the physical mechanism giving rise to the variation it is hard to determine this component's contribution to a potential isotropic background.

Another problem arises from the interpolation of a model derived from the broadband DIRBE observations to the narrow-band NIRS observations. Matsumoto et al. (2005) needed adjustment factors as large as 25% to get the Kelsall model to fit at some wavelengths. This suggests potential errors in the model that are similar to the levels of the residual emission.

The greatest cause for concern is created by the fact that if we subtract the resolved extragalactic emission (EBL2) from the isotropic residual found by Matsumoto et al. (2005), then a simple scaling of their own zodiacal component produces an excellent fit to the residual emission. Figure 2 shows the spectrum of the total sky intensity, the integrated starlight, and the residual isotropic component, all normalized to the zodiacal light spectrum. While neither the total sky brightness nor the starlight is exactly like the zodiacal light spectrum, the figure shows that the isotropic component found by Matsumoto et al. (2005) has

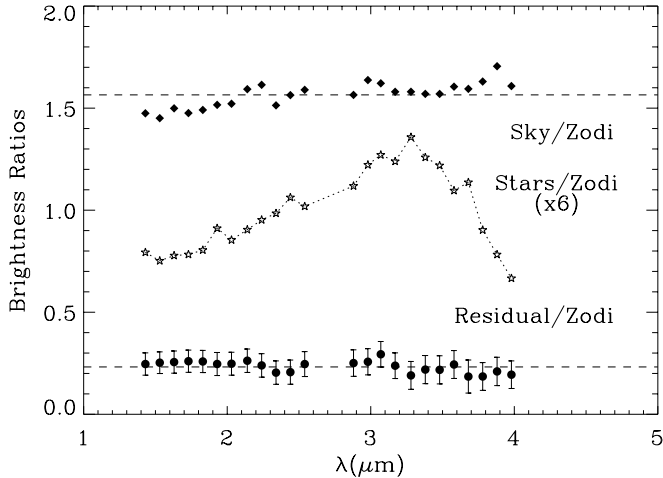


FIG. 2.—Spectrum of the total sky intensity, the integrated Galactic starlight, and the residual isotropic component, all normalized to the zodiacal light (ZL) spectrum. Starting from the observed sky spectrum, which differs from that of the ZL, the subtraction of the contribution from Galactic stars, which is dramatically different from the ZL spectrum, leads to a residual spectrum that is very well matched by that of the ZL. The residual spectrum represents 23.2% of the total ZL intensity.

a spectrum that is well matched by zodiacal light ($\chi^2 = 0.21$). Thus, the 0.232 mean ratio of the isotropic/zodiacal intensity may imply a missing component of the zodiacal light model which, if truly isotropic, would increase the zodiacal light intensity by $\sim 25\%$ at ecliptic latitudes $\beta \approx 50$ and by smaller amounts at lower latitudes.

The existence of such a large missing isotropic component of the zodiacal light is quite significant, but should not be totally surprising. Kelsall et al. (1998) showed that at the north Galactic pole ($\beta = 30$) the use of three alternate kernels for the geometry of the main IPD cloud can change the $2.2 \mu\text{m}$ zodiacal light intensity by up to 14%. There is no certainty that there are no other models with different geometries or additional components that may provide good fits to the temporal variations observed by DIRBE while producing even larger mean brightnesses (and lowering the level of any residual emission). This sort of systematic uncertainty is the most important for CIB studies, and it is also the hardest to estimate, because of the difficulty in measuring the absolute brightness of the zodiacal light alone.

One observation that could eliminate these uncertainties in the absolute intensity of the zodiacal light is the measurement of scattered solar absorption lines at near-IR wavelengths. Comparison of the relative depths of the lines in the solar and in the zodiacal spectrum can reveal the absolute intensity of the zodiacal light. Such measurements have been made in the optical by the Wisconsin $H\alpha$ Mapper (WHAM), which has measured the profile of the scattered solar $\text{Mg I } \lambda 5184$ absorption line in the zodiacal light (Reynolds et al. 2004).

In summary, the NIRBL at $1.2 \mu\text{m} < \lambda < 4 \mu\text{m}$ can be very well fit by a zodiacal dust spectrum, which is actually a nominally better fit than those of the Population III models presented later in this paper. However, current observations suggest that the NIRBL spectrum drops significantly at wavelengths below $\sim 1 \mu\text{m}$. It is very unlikely that the zodiacal emission contains such a discontinuity in the reflected solar spectrum. Consequently, if the apparent drop in the NIRBL spectrum is real, then an alternative nonlocal source is needed to account for its origin. In the following, we therefore assume that the NIRBL is extragalactic and examine the implication of its spectral shape and

intensity for the formation of the first luminous objects in the universe.

3. A COSMOLOGICAL ORIGIN OF THE EXCESS EMISSION

3.1. Global Energetics and Metallicity Considerations

Before pursuing more detailed modeling, it is instructive to estimate the cosmic energy release required to account for the total NIRBL intensity. We assume that the comoving luminosity density is given by

$$j(z) = j(z_f) \left(\frac{1+z}{1+z_f} \right)^{-2}, \quad (1)$$

where z_f is the redshift corresponding to the last epoch of this energy release. The total EBL intensity is given by

$$I_{\text{EBL}} = \frac{c}{4\pi} \int_{z_f}^{\infty} j(z) \left| \frac{dt}{dz} \right| \frac{dz}{1+z}, \quad (2)$$

where

$$\left| \frac{dt}{dz} \right| = H_0^{-1} [(1+z)E(z)]^{-1},$$

$$E(z) \equiv [\Omega_{\Lambda} + (1+z)^3 \Omega_m]^{1/2}. \quad (3)$$

Figure 3 depicts the value of $j(z_f)$ needed to produce a given background intensity for different values of z_f . The integrated NIRBL intensity is $30 \text{ nW m}^{-2} \text{ sr}^{-1}$ in the $\sim 1.4\text{--}4 \mu\text{m}$ NIRS wavelength region. The figure shows that for $6 < z_f < 9$, a luminosity density of $j = (0.7\text{--}1.8) \times 10^{11} L_{\odot} \text{ Mpc}^{-3}$ is needed to reproduce this intensity. Smaller values of z_f need lower luminosity densities. We note that in this exercise only the $1.4\text{--}4 \mu\text{m}$ NIRBL intensity is being considered. Later, we present more detailed models of Population III emission that produce emission outside this wavelength range and thus lead to somewhat larger intensities and luminosity densities.

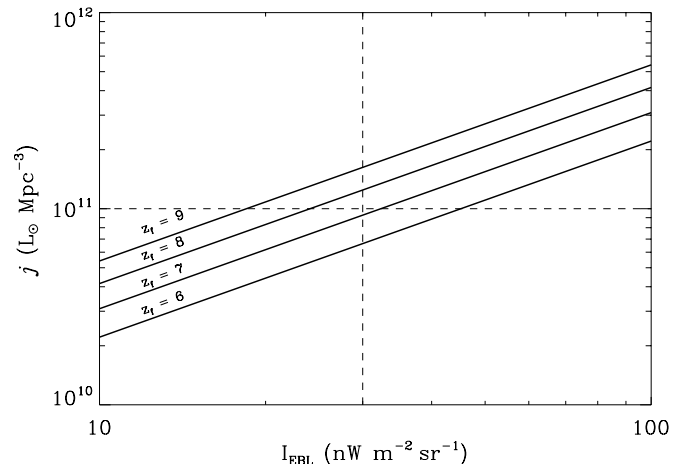


FIG. 3.—Comoving luminosity density needed to produce a given EBL intensity, for different values of z_f , the final epoch of energy injection. The luminosity density was assumed to have a $(1+z)^{-2}$ dependence at $z > z_f$. Calculations for different values of z_f are represented by solid lines. The vertical dashed line corresponds to the value of the NIRBL intensity integrated over the $1.4\text{--}4 \mu\text{m}$ interval.

Released over an effective period of Δt , the corresponding comoving energy density is

$$\epsilon(\text{ergs Mpc}^{-3}) \equiv j\Delta t, \quad (4)$$

where

$$\Delta t \equiv \int_{z_f}^{\infty} \frac{j(z)}{j(z_f)} \left| \frac{dt}{dz} \right| dz. \quad (5)$$

Values of Δt for $z_f = \{6, 7, 9\}$ are $\Delta t(\text{Myr}) = \{413, 339, 242\}$, giving

$$\epsilon(\text{ergs Mpc}^{-3}) = \begin{cases} 3.4 \times 10^{60} & \text{for } z_f = 6, \\ 3.6 \times 10^{60} & \text{for } z_f = 7, \\ 5.2 \times 10^{60} & \text{for } z_f = 9. \end{cases} \quad (6)$$

The release of this energy density by hydrogen burning in stars converts a comoving mass density

$$\rho_M \equiv \frac{\epsilon}{\eta c^2} \approx 3.2 \times 10^8 M_{\odot} \text{ Mpc}^{-3} \quad (7)$$

of hydrogen into helium and heavier elements, where $\eta = 0.007$ is the energy conversion efficiency for nuclear energy-generating reactions. Injected into the intergalactic medium at redshifts ≥ 7 , this creates an early enrichment of

$$-\Delta X = \Delta Y + \Delta Z = \frac{\rho_M}{\rho_b} \approx 0.052, \quad (8)$$

where X , Y , and Z are, respectively, the cosmic mass fractions of hydrogen, helium, and heavier elements and $\rho_b = 6.0 \times 10^9 M_{\odot} \text{ Mpc}^{-3}$ is the comoving baryonic density. This value is comparable to the current enrichment in helium ($\Delta Y \approx 0.04$) and heavy elements ($\Delta Z \approx 0.02$) since the big bang, leaving no room for significant production of metals by Population II and I stars.

To avoid this early overproduction of He and metals, it has been suggested by various authors (e.g., SBK02) that Population III stars should be very massive objects with masses above $260 M_{\odot}$ that collapse directly into a black hole at the end of their lifetime (Heger et al. 2003). These suggestions are also supported by models showing that Population III stars could have been more massive than present-day stars because of the inefficient fragmentation of the primordial condensations (Kashlinsky & Rees 1983; Bromm & Larson 2004). We therefore assume that the Population III stars giving rise to the NIRBL are sufficiently massive that they directly form black holes at the end of their lifetimes. The added advantage of these massive stars is that they are fully convective and that over their lifetimes they convert all their initial hydrogen into helium and heavier elements. Therefore, they require the minimal amount of baryons to be incorporated into stars in order to generate the required NIRBL intensity. The baryonic mass fraction that needs to be converted into stars is then given by

$$f_b = \frac{\epsilon}{\eta \rho_b c^2} = \frac{\rho_M}{\rho_b} \approx 0.052 = -\Delta X. \quad (9)$$

This corresponds to a comoving stellar mass density of

$$\rho_* = \rho_M = 3.2 \times 10^8 M_{\odot} \text{ Mpc}^{-3}. \quad (10)$$

Generated over an effective period of Δt , this gives a mean comoving star formation rate (SFR) of $\sim 1 M_{\odot} \text{ yr}^{-1} \text{ Mpc}^{-3}$.

All rates and densities derived above are larger by factors of 2–4 than those derived from models in which Population III stars form at a rate proportional to the collapse rate of halos in a cold dark matter (CDM) universe with a star formation efficiency of about 40% (Bromm & Loeb 2002; Madau & Silk 2005). However, the discrepancies may be even larger because (1) the SFR derived above represents a *lower limit* on the formation rate of Population III stars that is required to generate the NIRBL intensity, since it assumes that all the mass incorporated into stars is transmuted by nuclear reactions into heavier elements, and (2) the NIRBL intensity included only the radiation detected in the 1.4–4 μm band, and any emission from Population III stars outside this band increases the required energy production and SFRs. In the following we present more detailed models of the contribution of Population III stars to the EBL.

3.2. Models of Emission from Population III Stars

3.2.1. Stellar Parameters

Calculations are considerably simplified when all stars have masses M in excess of $\sim 100 M_{\odot}$, beyond which stars are dominated by radiation pressure. Their luminosity is approximately given by the Eddington limit, $L_{\text{Edd}}/L_{\odot} = 3.3 \times 10^4 M/M_{\odot}$; their effective temperature is roughly independent of mass and approximately equal to 10^5 K (Bond et al. 1984); their spectrum is characterized by that of a blackbody at that temperature (Bromm et al. 2001); and their lifetime, given by $\tau_* = \epsilon M c^2 / L \approx 3.2 \times 10^6 \text{ yr}$, is independent of the stellar mass. Furthermore, if they have masses in excess of $260 M_{\odot}$, they end their lives as collapsed objects, preventing the overproduction of metals at high redshifts. For the purpose of our study, we adopt the same stellar parameters as those used in the study of SBK02: a stellar mass of $M_* = 10^3 M_{\odot}$, yielding a luminosity $L_* = 3.3 \times 10^7 L_{\odot}$, and a stellar spectrum characteristic of a 10^5 K blackbody.

3.2.2. The Spectrum of an Ionization-bounded Primordial H II Region

The ionizing photons emanating from the stars can either be absorbed in the remnant nebula from which the stars formed or escape into the IGM if the nebula is not massive enough. As shown by SBK02, the two cases leave different imprints on the NIRBL. A larger EBL intensity is generated when all the ionizing photons are assumed to be locally absorbed compared to the case in which the ionizing radiation escapes into the IGM. In the following we assume that all the ionizing photons are locally absorbed, creating an ionization-bounded H II region around the star. Given a NIRBL intensity, this assumption leads to a lower limit on the Population III SFR.

We used CLOUDY (Ferland 1996) to calculate the spectral signature of a Population III star and its surrounding H II region, assuming that all the stellar ionizing photons are absorbed in the surrounding nebula. The nebula was assumed to have primordial composition (H and He mass fractions of 0.76 and 0.24, respectively) and a hydrogen number density of 10^4 cm^{-3} . The radiation emerging from the nebula comprises three spectral components: (1) a stellar continuum component consisting of photons that were not absorbed by the ambient gas, (2) a nebular continuum emission component, and (3) a nebular line emission component. The emission lines emerging from the H II regions are scattered by the ambient IGM, and we have used the SBK02 approximation (their eq. [15]) to calculate the line profile originally derived from Monte Carlo simulations by Loeb & Rybicki (1999). Figure 4 depicts the three emission components in the rest-frame of the star, assumed (for the purpose of calculating the scattered line profile) to have formed at $z = 15$.

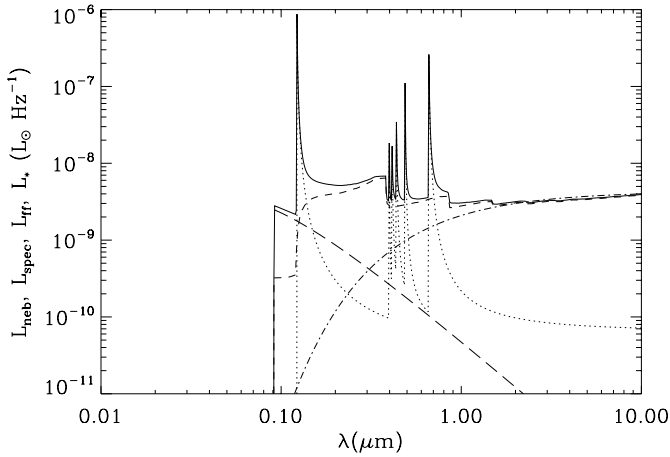


FIG. 4.—Components of the Population III source spectrum. (1) Escaping nonionizing stellar radiation (L_ν^* ; *long-dashed line*), (2) nebular continuum emission (L_ν^{cont} ; *short-dashed line*), and (3) nebular line emission (L_ν^{lines} ; *dotted line*), represented here by the Ly α and Balmer series recombination lines. Also shown in the figure is the free-free contribution (*dash-dotted line*) to the nebular continuum emission component. The source luminosity was calculated for a $10^3 M_\odot$ star radiating at the Eddington luminosity with a blackbody spectrum at $T = 10^5$ K. Line spectra were broadened to account for scattering in the IGM, assuming an injection epoch of $z = 15$. Total luminosities in each component are presented in Table 1.

The mass of the ionized nebula is about $1.4 \times 10^4 M_\odot$, which is the minimum mass required to create an ionization-bounded H II region for the given stellar parameters. This implies a star formation efficiency $\eta_* \approx 1/(1 + 1.4) \approx 0.41$. The H II region is therefore ionization bounded for $\eta_* \lesssim 0.41$. Table 1 presents the parameters of the H II region relevant to our calculations.

3.2.3. Global Parameters

At electron densities of 10^4 cm^{-3} the recombination timescales are short compared to the stellar lifetime of $\tau_* \approx 2 \times 10^6$ yr. The creation of the NIRBL requires therefore the continuous formation of stellar objects over a yet to be determined redshift interval $[z_{\text{min}}, z_{\text{max}}]$. The contribution of the star and H II region then creates a spectrum with an intensity

$$\nu I_\nu(\nu) = \frac{c}{4\pi} \times \int_{z_{\text{min}}}^{z_{\text{max}}} n_*(z) [L_\nu^*(\nu', z) + L_\nu^{\text{cont}}(\nu', z) + L_\nu^{\text{lines}}(\nu', z)] \left| \frac{dt}{dz} \right| dz, \quad (11)$$

where the terms in the square brackets represent, respectively, the spectral luminosity density ($L_\odot \text{ Hz}^{-1}$) of the escaping stellar, nebular continuum, and line emission components, $\nu' \equiv \nu(1+z)$ is the frequency of the emitted photon and ν is its observed one, and $n_*(z)$ is the comoving number density of Population III stars, assumed to have a z -dependence of the form

$$n_*(z) = n_0 \left(\frac{1+z}{1+z_{\text{min}}} \right)^\alpha. \quad (12)$$

The limiting redshifts z_{min} and z_{max} , n_0 , and α are adjustable parameters chosen to give the best fit of the model spectrum to the observed NIRBL.

To illustrate the sensitivity of the NIRBL spectrum to the model input parameters, we calculated $\nu I_\nu(\nu)$ for several values of z_{min} and z_{max} . All models were calculated for a value of

TABLE 1
STELLAR AND NEBULAR ENERGETICS

Emission Component	Luminosity (L_\odot)	Temperature (K)
Input radiation:		
Stellar	3.3×10^7	1.0×10^5
Escaping radiation:		
Stellar	3.48×10^6	...
Nebular (continuum + free-free)	9.37×10^6	2.2×10^4
Nebular lines:		
Ly α (0.122 μm)	1.68×10^7	...
H α (0.656 μm)	1.02×10^6	...
H β (0.486 μm)	3.38×10^5	...
H γ (0.434 μm)	1.58×10^5	...
H δ (0.410 μm)	8.33×10^4	...
H ϵ (0.397 μm)	5.15×10^4	...

NOTES.—The stellar luminosity was calculated for a $M_* = 10^3 M_\odot$ star radiating at the Eddington luminosity. Nebular energetics were calculated by CLOUDY for a nebula with primordial composition and a hydrogen number density of 10^4 cm^{-3} . The total mass of the ionization-bounded H II region is $1.4 \times 10^3 M_\odot$.

$\alpha = -2.0$, which provided a good fit to the slope of the NIRBL spectrum. For each choice of z_{min} and z_{max} , n_0 is determined by a least-squares fit to the NIRBL. Calculations were performed for three values of z_{min} : the lowest value, $z_{\text{min}} = 6$, was chosen so that the short-wavelength edge of the redshifted Ly α line is just above the EBL determination of Bernstein et al. (2002). This choice of z_{min} has the added attractive feature of redshifting the H α line into the 4.9 μm DIRBE bandpass. A maximum value of $z_{\text{min}} = 9$ was chosen so that the edge of the Ly α line coincides with the 1.25 μm EBL intensity, and finally, calculations were also performed for an intermediate value of $z_{\text{min}} = 7$. Salvaterra & Ferrara (2003a) obtained a “hard” limit of $z_{\text{min}} = 8.8$, motivated by the apparent drop in NIRBL between the NIRS data and the DIRBE J (1.25 μm) band intensity. However, the drop in the EBL intensity at this wavelength is statistically insignificant and should not be used to constrain the value of z_{min} . The value of z_{max} was varied from 15 to a maximum value of 30, since model results did not vary significantly for larger redshifts.

3.3. Model Results

Figure 5 summarizes the results of our calculations. All panels display the three EBL spectra that can be attributed to star formation at $z \lesssim 5$. Also shown in the figure are the spectral contribution of the nonionizing stellar (*long-dashed lines*), the nebular continuum (*short-dashed lines*), and the nebular line (*dotted lines*) emission components to the NIRBL intensity. The thick solid line represents the sum of these emission components added to the EBL2 intensity. In addition to the values of z_{min} and z_{max} , the figures also give the value of n_0 in Mpc^{-3} and the reduced χ^2 of the fit to the NIRS data points.

The two top panels of Figure 5 show the results for $z_{\text{min}} = 6$. In spite of the attractive result that the model can account for the upturn of the DIRBE 4.9 μm intensity, it otherwise provides a poor fit to the NIRBL at shorter wavelengths. The bottom two panels of Figure 5 depict the resulting Population III spectra for $z_{\text{min}} = 9$ and different choices of z_{max} . For this value of z_{min} , none of the Balmer lines contribute significantly to the 4.9 μm intensity. The H β line falls in that wavelength band; however, the line intensity and the intensity of the nebular emission are significantly reduced compared to those in the $z_{\text{min}} = 6$ case, because the epoch of their formation has been shifted to higher

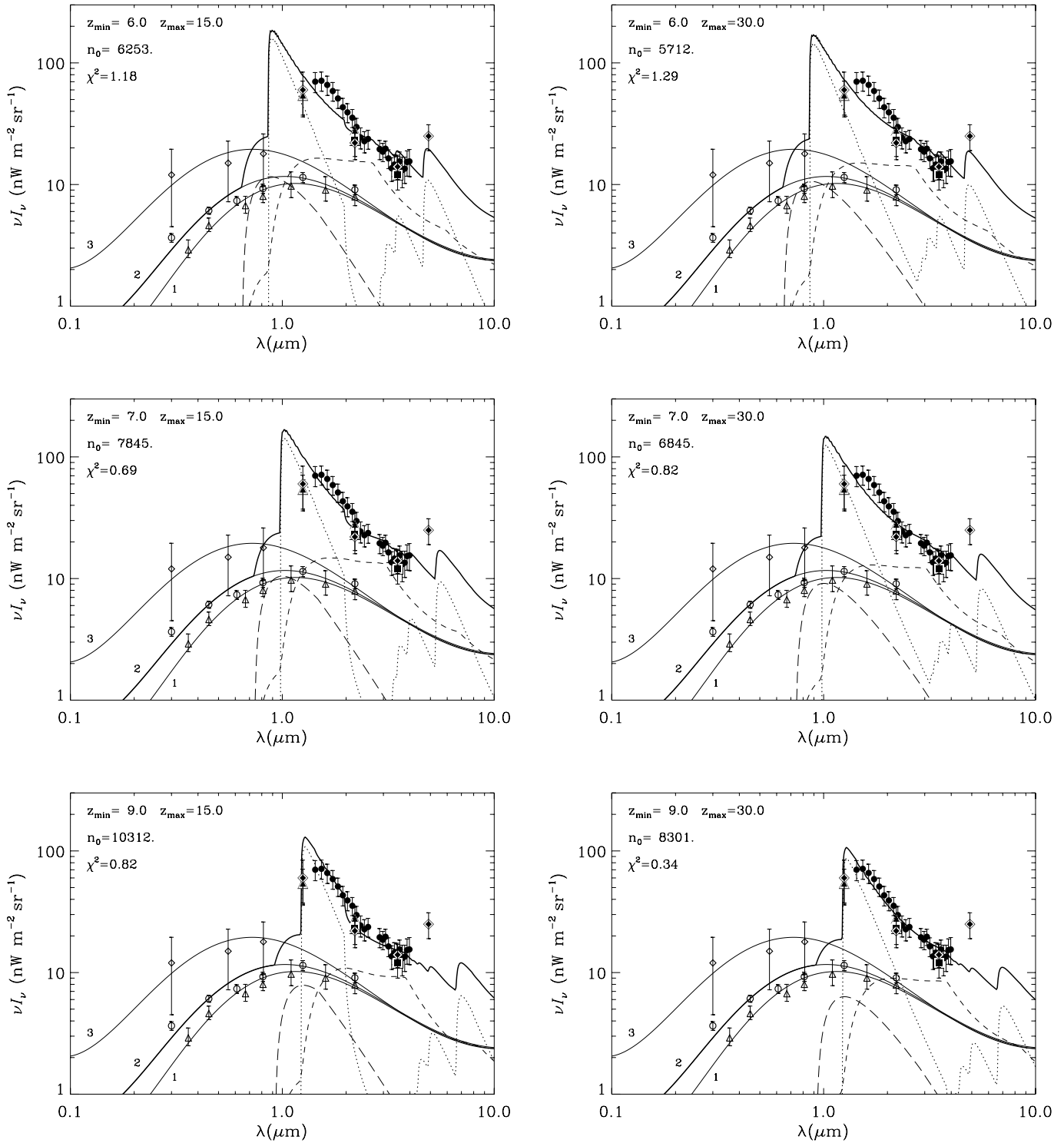


FIG. 5.—Imprint of Population III stars on the near-IR EBL for different values of $[z_{\min}, z_{\max}]$. Curves labeled “1,” “2,” and “3” are different fits to the EBL formed by normal star-forming galaxies. The heavy solid line represents the sum of all three components of the Population III contribution and EBL2. Also shown in the figure are the three Population III emission components: the nonionizing photons escaping from the nebula (*long-dashed line*), the nebular continuum and free-free emission (*short-dashed line*), and the nebular line emission (*dotted line*). All models were calculated for a SFR $n_*(z) = n_0[(1+z)/(1+z_{\min})]^\alpha$, with $\alpha = -2.0$. The value of n_0 is given in units of Mpc^{-3} .

redshifts. Consequently, the Population III spectrum never contributes significantly to the $4.9 \mu\text{m}$ emission. For $z_{\max} = 15$, the long-wavelength edge of the $\text{Ly}\alpha$ line occurs around $2 \mu\text{m}$, and the spectrum drops somewhat below the observed NIRBL. A value of $z_{\max} = 30$ provides a somewhat better fit to the data. This case illustrates the importance of the NIRS wavelength

coverage in constraining the high- z end of the redshift interval. With only the DIRBE data, both fits would seem equally acceptable. The two middle panels of Figure 5 show the model results for $z_{\min} = 7$, and different values of z_{\max} . The figures show an improvement in the fit as z_{\max} decreases from 30 to 15. Overall, the best fits to the NIRBL are provided by the following

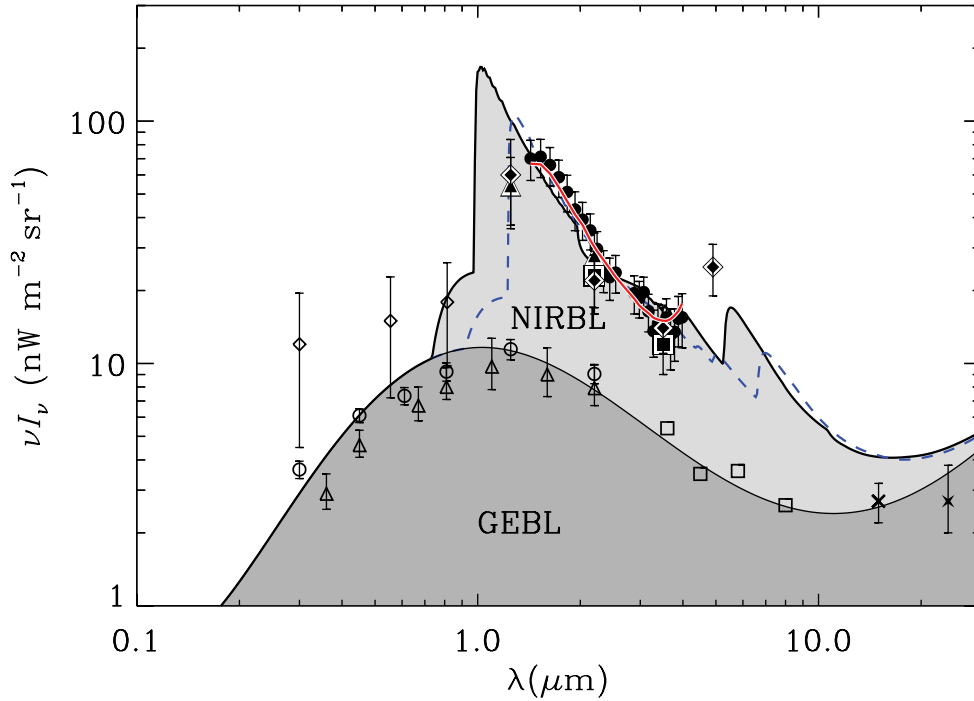


FIG. 6.—Comparison of current limits and detections of the extragalactic background light (EBL) to the spectrum generated by normal star-forming galaxies (GEBL = EBL2 in Fig. 1; dark shaded area) and the excess near-IR background light (NIRBL; lightly shaded area). The limits and detections are based on data and analyses including ground- and space-based measurements summarized by Hauser & Dwek (2001), with additional data from Matsumoto et al. (2005), Cambrésy et al. (2001), Fazio et al. (2004), and Papovich et al. (2004). The open circles represent extrapolated galaxy number counts (Totani et al. 2001). The solid blue line represents the sum of the Population III model NIRBL7 and the GEBL, and the dashed blue line, that of model NIRBL9 plus the GEBL. The red curve depicts the spectrum of the zodiacal light (Matsumoto et al. 2005), scaled by a factor of 0.23 to provide a fit to the NIRS data.

models, designated NIRBL7 and NIRBL9, characterized by the following set of parameters:

$$\begin{aligned} & \{z_{\min}, z_{\max}, \alpha, n_0\} = \\ & \begin{cases} \{7, 15, -2.0, 7.8 \times 10^3 \text{ Mpc}^{-3}\} & \text{model NIRBL7,} \\ \{9, 30, -2.0, 8.3 \times 10^3 \text{ Mpc}^{-3}\} & \text{model NIRBL9.} \end{cases} \quad (13) \end{aligned}$$

Figure 6 depicts the spectral signature of the best fits of the different models to the NIRBL.

4. COSMOLOGICAL IMPLICATIONS

4.1. The Formation Rate of Population III Stars

Model fits to the NIRBL provide the comoving number density of Population III stars, $n_*(z)$ as a function of redshift. The formation rate, $\dot{\rho}_*(z)$, of Population III stars for $z \geq z_{\min}$ is given by

$$\begin{aligned} \dot{\rho}_*(z) &= n_*(z) \frac{M_*}{\tau_*} \\ &= n_0 \frac{M_*}{\tau_*} \left(\frac{1+z}{1+z_{\min}} \right)^{-2} \\ &\equiv \dot{\rho}_0 \left(\frac{1+z}{1+z_{\min}} \right)^{-2}. \end{aligned} \quad (14)$$

Figure 7 compares the formation rate of Population III stars for the two different Population III formation scenarios to that of stars in normal galaxies, for the model output parameters given in Figure 5 (see also Table 2). The figure shows that the formation rate of Population III stars is higher by a factor of 10 than the SFR in normal galaxies, with an abrupt drop around the reionization redshift z_{\min} .

In the hierarchical model for structure formation in a CDM-dominated universe, galaxies form out of the cooling gas streaming into the potential well of collapsed dark halos, which evolve with redshift through a series of hierarchical mergers. The SFR is then equal to the growth rate of the mass of collapsed halos that are above some critical mass, M_{crit} , times the product of the fraction of the total mass of dark matter that is in baryonic form and the star formation efficiency η_* . The latter quantity depends on details of the state (ionized, atomic, or molecular) of the primordial gas and, for later generations of stars, the metallicity of the gas. Bromm & Loeb (2002) derived peak SFRs between ~ 0.3 and $0.6 M_\odot \text{ yr}^{-1} \text{ Mpc}^{-3}$, depending on the phase (atomic

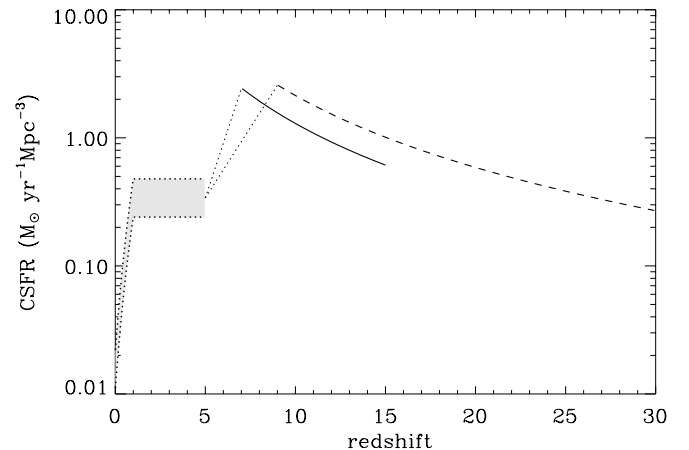


FIG. 7.—SFR due to normal galaxies (shaded area; see Gabasch et al. 2004 for references) and Population III stars. The solid and dashed lines represent models NIRBL7 and NIRBL9, respectively, and are characterized by model parameters given in eq. (6) and spectra given in Fig. 5.

TABLE 2
MODEL OUTPUT PARAMETERS

Emission Component	NIRBL7	NIRBL9
n_0 (Mpc^{-3}).....	7845	8301
Δt (Myr).....	309	238
$\dot{\rho}_*$ ($M_\odot \text{ yr}^{-1} \text{ Mpc}^{-3}$).....	2.45	2.59
ρ_0 ($M_\odot \text{ Mpc}^{-3}$).....	7.57×10^8	6.17×10^8
ρ_*/ρ_b	0.12	0.10
j_0 ($L_\odot \text{ Mpc}^{-3}$).....	2.60×10^{11}	2.74×10^{11}
ϵ_* (ergs Mpc^{-3}).....	9.7×10^{60}	7.9×10^{60}
\tilde{E}_b (ergs baryon $^{-1}$).....	1.33×10^{-6}	1.08×10^{-6}
(keV baryon $^{-1}$).....	820	670
I_{NIRBL} (nW $\text{m}^{-2} \text{sr}^{-1}$) ^a	74	46

NOTES.—Quantities were calculated for a Λ CDM model characterized by $\Omega_\Lambda = 0.73$, $\Omega_m = 0.27$, $\Omega_b = 0.044$, and a Hubble constant of $H_0 = 70 \text{ km s}^{-1}$. For these parameters, the current baryonic mass and number densities are $\rho_b = 6.0 \times 10^9 M_\odot \text{ Mpc}^{-3}$ and $n_b = 7.35 \times 10^{66} \text{ Mpc}^{-3}$, respectively. The effective time Δt is defined in eq. (5).

^a I_{NIRBL} represents the contribution of Population III stars to the EBL intensity, integrated over all wavelengths. Integration over only the $\sim 1.4\text{--}4.0 \mu\text{m}$ wavelength interval gives a value of only $\sim 30 \text{ nW m}^{-2} \text{sr}^{-1}$. This integration omits the lowest redshift Ly α emission (primarily for model NIRBL7) and all of the redshifted Balmer emission.

or molecular) of the collapsing gas, at $z \approx 10$. Our results show a similar functional behavior, but with a SFR larger by factors of 4–10, which is a direct consequence of attributing the NIRBL to the energy output from these stars.

4.2. The Fraction of Baryons Converted to Stars

The total comoving mass density of baryons converted to stars is given by $\rho_* = \dot{\rho}_0 \Delta t$, where Δt is given by equation (5). The fraction of baryons in the universe that need to be converted into Population III stars in order to account for the NIRBL intensity is given by ρ_*/ρ_b , which is equal to 10%–12% (see Table 2).

4.3. The Energy Released per Baryon

The total energy density emitted by the Population III stars in order to produce the NIRBL is given by

$$\epsilon_* \equiv j_0 \Delta t = n_0 L_* \Delta t, \quad (15)$$

which has an average value of $9 \times 10^{60} \text{ ergs Mpc}^{-3}$. Table 2 gives the value of ϵ_* for the two Population III formation scenarios. The value of \tilde{E}_b , the energy released by Population III stars per baryon in the universe, ranges from 670 to 820 keV baryon $^{-1}$.

4.4. The Ionization of the Intergalactic Medium by Population III Stars

Throughout this work we assumed that all the ionizing photons are absorbed in the surrounding nebula, with none escaping into the intergalactic medium. Such a scenario is inconsistent with the observational evidence that most of the IGM was ionized at $z \geq 7$. We therefore relax this assumption and calculate the fraction of the ionizing photons that need to escape the nebula in order to ionize the IGM at this redshift.

The number of ionizing Lyman continuum photons, N_{Lyc} , emitted by a star with a blackbody spectrum of temperature T and a luminosity L is given by

$$\frac{dN_{\text{Lyc}}}{dt} = \frac{15}{\pi^4} \frac{L}{kT} \int_{x_0}^{\infty} \frac{x^2 dx}{\exp(x) - 1} = 2.38 \times 10^{51} \text{ s}^{-1}, \quad (16)$$

where $x \equiv h\nu/kT$, $x_0 = x$ at the Lyman limit, and the last part of the equation was calculated for $L = 3.3 \times 10^7 L_\odot$ and $T = 10^5 \text{ K}$.

To keep most of the IGM ionized, a fraction of these photons need to leak out of the nebula, ionizing the surrounding medium so that the Strömgren spheres around these stars have a volume filling factor of about unity. For a perfectly uniform distribution of Population III stars, the average volume occupied by each star is given by $n_0^{-1} \approx 1/8000 \text{ Mpc}^3$. The injection rate of ionizing photons required to keep this volume fully ionized is given by

$$\frac{dN_{\text{ion}}}{dt} = n_i n_e \alpha V, \quad (17)$$

where $\alpha \approx 4 \times 10^{-13} \text{ cm}^3 \text{ s}^{-1}$ is the recombination factor calculated for a gas temperature of 10^4 K and n_i and n_e are, respectively, the number density of ions and electrons of the medium. The baryonic number density at $z = 7$ is $n_b = 1.3 \times 10^{-4} \text{ cm}^{-3}$. So, for a fully ionized IGM we get

$$\frac{dN_{\text{ion}}}{dt} = 2.5 \times 10^{49} \text{ s}^{-1}. \quad (18)$$

Comparing to the production rate of ionizing photons given by equation (16), we find that for a uniform distribution of Population III stars, only 1% of the ionizing stellar photons need to escape the nebula in order to create a fully ionized IGM. This small fraction has no noticeable effect on our calculations of the NIRBL, which assumed that all the ionizing photons are locally absorbed.

5. OTHER INSIGHTS INTO THE ORIGIN OF THE NIRBL

5.1. Spatial Fluctuations in the EBL

Random spatial fluctuations measured in the background emission for DIRBE, the Two Micron All Sky Survey (2MASS), and NIRS (Kashlinsky & Odenwald 2000; Kashlinsky et al. 2002; Matsumoto et al. 2005) have been presented as evidence for the extragalactic nature of the NIRBL (Magliocchetti et al. 2003). These fluctuations are found to be in excess of those expected from instrumental noise and local IPD or galactic stars and are even larger than the fluctuations expected from normal galaxy populations. On smaller spatial scales ($< 1^\circ$), the angular correlations or angular power spectra of these fluctuation are in rough agreement with models (Kashlinsky et al. 2004). However, as noted by Matsumoto et al. (2005) fluctuations on larger scales have amplitudes larger than those predicted by the present Population III models. It is therefore currently ambiguous whether the observed fluctuations provide evidence for or against the extragalactic nature of the NIRBL.

5.2. The Effect of the NIRBL on the Absorption-corrected TeV Spectrum of Blazars

Additional claims for the extragalactic nature of the NIRBL are based on the EBL opacity to very high energy γ -rays. The γ -ray photons from blazars interact with EBL photons, producing electron-positron pairs. The NIRBL, if extragalactic, therefore produces a discontinuity in the TeV opacity toward a blazar that, in principle, leaves its imprint on its intrinsic spectrum. Mapelli et al. (2004) have suggested that the observed S-shaped spectrum of H1426+428 is the manifestation of this absorption feature, assuming its intrinsic spectrum rises as $E^2 dN/dE \propto E^{0.4}$. However, an intrinsic spectrum in which $E^2 dN/dE \propto \text{const}$ provides an equally good fit to the observed spectrum when it is corrected for absorption by only the GEBL (Dwek et al. 2005). Thus, without accurate knowledge of the intrinsic γ -ray spectrum it is

impossible to confirm the extragalactic nature of the NIRBL. However, as shown below, it may be possible in specific cases to set limits on the nature of the NIRBL by examining the physical implications of the absorption-corrected spectrum.

The blazar PKS 2155–304 has been observed from over the entire optical to very high energy γ -ray wavelength regime. In particular, it has been observed by the Energetic Gamma-Ray Experiment Telescope (EGRET) on board the *Compton Gamma Ray Observatory* (Vestrand et al. 1995) at MeV-GeV energies and most recently by the High Energy Stereoscopic System (H.E.S.S.) experiment at TeV energies (Aharonian et al. 2005a). Compared to H1426+428, this blazar has a more accurately determined TeV γ -ray spectrum, well approximated by a power law. Although not all the ~ 10 eV–3 TeV data are contemporaneous, the entire nonthermal spectral energy distribution (SED) of PKS 2155–304 is well explained by the synchrotron self-Compton (SSC) model (Chiappetti et al. 1999), in which the blazar SED is characterized by a double peak: a synchrotron peak located at UV to X-ray energies (~ 0.1 –1 keV) and a Compton peak located at energies of about 3–300 GeV. The fit of the SSC model to the SED of PKS 2155–304 spanning the eV to TeV region of its energy spectrum is presented in Figure 8 of Chiappetti et al. (1999). Dwek et al. (2005; their Fig. 7) have shown that if the observed PKS 2155–304 spectrum is corrected for only GEBL absorption, then the resulting SED is characterized by a smooth parabolic function with a peak around 10 GeV, consistent with the SSC model presented by Chiappetti et al. (1999). In contrast, if corrected for the GEBL+NIRBL realization of the EBL, the blazar's SED exhibits a very steep rise with $E^2 dN/dE \propto E^{2.3}$ at TeV energies. In principle, it may be possible to reproduce a pileup of photons at TeV energies if these photons are produced by synchrotron emission from extremely high energy protons (Aharonian 2000). However, in this proton synchrotron model, even a steeply rising proton energy spectrum produces an intrinsic γ -ray spectrum that is only mildly increasing with energy (see, for example, Fig. 10 in Aharonian 2000). A pileup in the TeV spectrum of blazars can also be produced by the Comptonization of ambient optical radiation by an ultrarelativistic cold jet with a bulk motion Lorentz factor of $\sim 10^6$ – 10^7 emanating from the blazar (Aharonian et al. 2002). While such a scenario cannot be excluded, it is not likely to be the origin of the TeV emission from this blazar. The observed spectrum of this blazar is very well represented by a power law, and it requires a very fine tuning of its intrinsic spectrum to produce this power law with the additional TeV opacity generated by the NIRBL.

Alternatively, since the MeV-GeV EGRET and TeV H.E.S.S. data are not contemporaneous, it is possible that the SED has evolved in the time span between the observations so that the GEBL+NIRBL-corrected spectrum can be described by a simple SSC model, with a Compton peak at energies ≥ 2 TeV. However, as pointed out by Dwek et al. (2005), a shift in the Compton peak by about 2 orders of magnitude would require a similar shift in the synchrotron peak energy, which is not supported by repeated X-ray observations of this blazar.

The conclusions of Dwek et al. (2005) are corroborated by the recent detection of the most distant blazars H2356–309 ($z = 0.165$) and 1ES 1101–232 ($z = 0.186$; Aharonian et al. 2005b). Assuming that intrinsic blazar spectra steeper than

$E^2 dN/dE \propto E^{0.5}$ are physically unrealistic, Aharonian et al. (2005b) used these blazars to derive the strongest constraints on the EBL in the 0.8–4 μm wavelength region. The intensity they found is only slightly larger than that of the GEBL, leaving very little room for the contribution of Population III stars.

6. SUMMARY AND DISCUSSION

We have shown that attributing the entire NIRBL to the energy output from Population III stars, as suggested by Salvaterra & Ferrara (2003a), leads to several difficulties:

1. It requires a peak SFR of *at least* $\sim 1 M_{\odot} \text{ yr}^{-1} \text{ Mpc}^{-3}$, more likely about $2.5 M_{\odot} \text{ yr}^{-1} \text{ Mpc}^{-3}$, a value that is higher by a factor of 4–10 over that predicted from halo-collapse models.
2. It requires that about 10% of all baryons in the universe must be converted into Population III stars.
3. It predicts a γ -ray opacity leading to physically unrealistic absorption-corrected spectra of distant TeV blazars.

These difficulties suggest that at most only a small fraction of the NIRBL can be of extragalactic origin.

The spectrum of the NIRBL is almost identical to that of the zodiacal dust cloud. Therefore, the most plausible explanation for its origin is that it is reflected sunlight from the interplanetary dust cloud that, because of its isotropic spatial distribution, escaped detection by the DIRBE. However, such a component may also contribute to the thermal infrared emission at $\lambda \gtrsim 10 \mu\text{m}$, requiring a reassessment of the EBL detections at far-infrared wavelengths. Furthermore, spatial fluctuations in the NIRBL cannot be attributed to the zodiacal dust cloud, although regarding the many uncertainties in its detailed spatial structure, such a possibility cannot be entirely excluded.

Finally, we cannot exclude the possibility that the contribution of galaxies to the EBL may have been underestimated and that the EBL intensity at optical/near-IR wavelengths is significantly larger than the extrapolations of Totani et al. (2001). Deeper surveys with the *Spitzer* Infrared Array Camera will be able to provide improved data on the contribution of resolved galaxies to the EBL.

Alternatively, a completely different source of energy, gravitational rather than nuclear, may be the origin of the NIRBL excess (Bond et al. 1986; Madau & Silk 2005). Further 0.1–10 μm measurements of the absolute brightness of the sky and of the zodiacal dust cloud will be crucial for determining the true spectrum of the NIRBL, i.e., the magnitude and location of the redshifted Ly α break in the EBL spectrum, and for resolving the origin of the NIRBL. Experiments such as the Cosmic Infrared Background Experiment (CIBER, PI: J. Bock), with the objectives of measuring the EBL spectrum around 1 μm and its spatial fluctuations in the *I* (0.90 μm) and *H* (1.65 μm) bands, represent the next step in gaining further insight into the nature and origin of the NIRBL.

We thank Frédéric Galliano for running the CLOUDY code and an anonymous referee for constructive suggestions that led to substantial improvements in the manuscript. E. D. acknowledges the support of the NASA LTSA 2003.

REFERENCES

- Aharonian, F. A. 2000, *NewA*, 5, 377
 Aharonian, F. A., Timokhin, A. N., & Plyasheshnikov, A. V. 2002, *A&A*, 384, 834
 Aharonian, F. A., et al. 2005a, *A&A*, 430, 865
 ———. 2005b, *Nature*, submitted (astro-ph/0508073)
 Arendt, R. G., & Dwek, E. 2003, *ApJ*, 585, 305
 Arendt, R. G., et al. 1998, *ApJ*, 508, 74
 Barkana, R., & Loeb, A. 2001, *Phys. Rep.*, 349, 125
 Bennett, C. L., et al. 2003, *ApJS*, 148, 1

- Bernstein, R. A., Freedman, W. L., & Madore, B. F. 2002, *ApJ*, 571, 56
- Bond, J. R., Arnett, W. D., & Carr, B. J. 1984, *ApJ*, 280, 825
- Bond, J. R., Carr, B. J., & Hogan, C. J. 1986, *ApJ*, 306, 428
- Bromm, V., Kudritzki, R. P., & Loeb, A. 2001, *ApJ*, 552, 464
- Bromm, V., & Larson, R. B. 2004, *ARA&A*, 42, 79
- Bromm, V., & Loeb, A. 2002, *ApJ*, 575, 111
- Cambresy, L., Reach, W. T., Beichman, C. A., & Jarrett, T. H. 2001, *ApJ*, 555, 563
- Chiappetti, L., et al. 1999, *ApJ*, 521, 552
- Cooray, A., Bock, J. J., Keating, B., Lange, A. E., & Matsumoto, T. 2004, *ApJ*, 606, 611
- Cooray, A., & Yoshida, N. 2004, *MNRAS*, 351, L71
- Dwek, E., & Arendt, R. G. 1998, *ApJ*, 508, L9
- Dwek, E., Krennrich, F., & Arendt, R. G. 2005, *ApJ*, 634, 155
- Fan, X., et al. 2000, *AJ*, 120, 1167
- . 2001, *AJ*, 122, 2833
- Fazio, G. G., et al. 2004, *ApJS*, 154, 39
- Ferland, G. J. 1996, *HAZY*, A Brief Introduction to CLOUDY (Lexington: Univ. Kentucky Dept. Phys. Astron. Internal Rep.)
- Gabasch, A., et al. 2004, *ApJ*, 616, L83
- Glover, S. 2005, *Space Sci. Rev.*, 117, 445
- Gorjian, V., Wright, E. L., & Chary, R. R. 2000, *ApJ*, 536, 550
- Haiman, Z., & Loeb, A. 1997, *ApJ*, 483, 21
- Hauser, M. G., & Dwek, E. 2001, *ARA&A*, 39, 249
- Hauser, M. G., et al. 1998, *ApJ*, 508, 25
- Heger, A., Fryer, C. L., Woosley, S. E., Langer, N., & Hartmann, D. H. 2003, *ApJ*, 591, 288
- Kashlinsky, A. 2005, *Phys. Rep.*, 409, 361
- Kashlinsky, A., Arendt, R. G., Gardner, J. P., Mather, J. C., & Moseley, H. S. 2004, *ApJ*, 608, 1
- Kashlinsky, A., & Odenwald, S. 2000, *ApJ*, 528, 74
- Kashlinsky, A., Odenwald, S., Mather, J., Skrutskie, M. F., & Cutri, R. M. 2002, *ApJ*, 579, L53
- Kashlinsky, A., & Rees, M. J. 1983, *MNRAS*, 205, 955
- Kelsall, T., et al. 1998, *ApJ*, 508, 44
- Kogut, A., et al. 2003, *ApJS*, 148, 161
- Lagache, G., Haffner, L. M., Reynolds, R. J., & Tufte, S. L. 2000, *A&A*, 354, 247
- Loeb, A., & Barkana, R. 2001, *ARA&A*, 39, 19
- Loeb, A., & Rybicki, G. B. 1999, *ApJ*, 524, 527
- Madau, P., & Pozzetti, L. 2000, *MNRAS*, 312, L9
- Madau, P., & Silk, J. 2005, *MNRAS*, 359, L37
- Magliocchetti, M., Salvaterra, R., & Ferrara, A. 2003, *MNRAS*, 342, L25
- Mapelli, M., Salvaterra, R., & Ferrara, A. 2004, *NewA*, in press (astro-ph/0410615)
- Matsumoto, T. 2005, *ApJ*, 626, 31
- Metcalf, L., et al. 2003, *A&A*, 407, 791
- Papovich, C., et al. 2004, *ApJS*, 154, 70
- Reynolds, R. J., Madsen, G. J., & Moseley, S. H. 2004, *ApJ*, 612, 1206
- Salvaterra, R., & Ferrara, A. 2003a, *MNRAS*, 339, 973
- . 2003b, *MNRAS*, 340, L17
- Santos, M. R., Bromm, V., & Kamionkowski, M. 2002, *MNRAS*, 336, 1082 (SBK02)
- Scannapieco, E., Schneider, R., & Ferrara, A. 2003, *ApJ*, 589, 35
- Totani, T., Yoshii, Y., Iwamuro, F., Maihara, T., & Motohara, K. 2001, *ApJ*, 550, L137
- Vestrand, W. T., Stacy, J. G., & Sreekumar, P. 1995, *ApJ*, 454, L93
- Wright, E. L. 1998, *ApJ*, 496, 1
- . 2001, *ApJ*, 553, 538
- Wright, E. L., & Reese, E. D. 2000, *ApJ*, 545, 43

Note added in proof.—After the submission of this paper, we became aware of a study by E. Fernandez & E. Komatsu (astro-ph/0508174), who pointed out that if the NIRBL has a stellar origin, its formation need not be limited to metal-free Population III stars, but could also include the contribution from stars with significant metallicity.